

1 **A global analysis of reconstructed land climate changes during Dansgaard-** 2 **Oeschger events**

3 Mengmeng Liu^{1,2,*}, Iain Colin Prentice¹, Sandy P. Harrison²

4 1: Georgina Mace Centre for the Living Planet, Department of Life Sciences, Imperial College
5 London, Silwood Park Campus, Buckhurst Road, Ascot SL5 7PY, UK

6 2: Department of Geography and Environmental Science, University of Reading, Reading,
7 RG6 6AB, UK

8 *** Corresponding author: m.liu18@imperial.ac.uk**

9 Ms for: *Climate of the Past*

10 **Abstract**

11 Dansgaard–Oeschger (D–O) warming events are comparable in magnitude and rate to the
12 anticipated 21st century warming. As such, they provide a good target for evaluation of the
13 ability of state-of-the-art climate models to simulate rapid climate changes. Despite the wealth
14 of qualitative information about climate changes during the D–O events, there has been no
15 attempt to date to make quantitative reconstructions globally. Here we provide reconstructions
16 of seasonal temperature changes and changes in plant-available moisture across multiple D–O
17 events during Marine Isotope Stage 3 based on available pollen records across the globe. These
18 reconstructions show that the largest warming occurred in northern extratropics, especially
19 Eurasia, while western North America and the southern extratropics were characterised by
20 cooling. The change in winter temperature was significantly larger than the change in summer
21 temperature in the northern extratropics, indicating that the D–O warming events were
22 characterised by reduced seasonality, but there is no significant difference between the summer
23 and winter temperature changes in the southern extratropics. The antiphasing between northern
24 and southern extratropical changes, and the west-east pattern of cooling and warming in North
25 America are consistent across the eight D–O events examined, although the signal at individual
26 sites may vary between events. Globally, changes in moisture were positively correlated with
27 changes in temperature, but the strength and the sign of this relationship vary regionally. These
28 reconstructions can be used to evaluate the spatial patterns of changes in temperature and

- 29 moisture in the transient simulations of the D-O events planned as part of the Palaeoclimate
30 Modelling Intercomparison Project.

31 1. Introduction

32 Dansgaard–Oeschger (D–O) events are characterised in Greenland by a transition from cold
33 Greenland Stadial (GS) to warmer Greenland Interstadial (GI) conditions (Dansgaard et al.,
34 1993). The surface air temperature in Greenland increased by 10–15° C during the warming
35 phases; these warming events occur over an interval of between 50 and 200 years (Huber et
36 al., 2006; Kindler et al., 2014). Thus, the D-O events offer a parallel in terms of speed to
37 projected future warming, although both the baseline state and the mechanism inducing this
38 warming differ from anticipated 21st century climate changes. D-O events could therefore
39 provide an opportunity to determine how well climate models that are used for future
40 projections can simulate rapid climate changes (Malmierca-Vallet et al., 2023), particularly
41 regional patterns of warming (and cooling) that are regarded as a challenge for modelling
42 (Doblas-Reyes et al., 2021; Lee et al., 2021) and are highly important in assessing the
43 vulnerability of human societies to future climate changes (IPCC 2022).

44 D-O events are registered globally (Voelker, 2002; Sánchez Goñi and Harrison, 2010; Harrison
45 and Sánchez Goñi, 2010; Sánchez Goñi et al., 2017; Adolphi et al., 2019; Corrick et al., 2020).
46 Shifts in vegetation types between GI and GS states have been interpreted as primarily a
47 temperature signal in the extratropics and a moisture signal in the tropics (Harrison and
48 Sánchez Goñi, 2010). Speleothem records provide a good time-control on the synchronicity of
49 climate changes globally with the D-O events registered in Greenland (Adolphi et al., 2019;
50 Corrick et al., 2020), but the driver of this signal can either be temperature or precipitation
51 depending on the region. There are quantitative climate reconstructions based on terrestrial
52 pollen records from La Grande Pile (Guiot et al., 1993), Lago Grande di Monticchio (Huntley
53 et al., 1999), Padul (Camuera et al., 2022), El Cañizar de Villarquemado (Wei et al., 2021;
54 Camuera et al., 2022) and Lake Ohrid (Sinopoli et al., 2019), marine cores in the western
55 Mediterranean and offshore from Portugal (Sánchez-Goñi et al., 2002), diatom assemblages at
56 Les Echets, France (Ampel et al., 2010), bacterial membrane lipid records from the Eifel region
57 (Zander et al., 2023), isotopic measurements of earthworm calcite from the Rhine Valley
58 (Prud'homme et al., 2022) and clumped isotope measurements on snails in Hungary (Újvári et
59 al., 2021). Aside from the lack of comparable quantitative estimates from outside Europe,
60 differences in the methodology employed and in the specific climate variables reconstructed in
61 each of these studies limits their usefulness for model evaluation. In particular, given that there
62 is still uncertainty as to whether the D-O cycles are characterised by changes in seasonality

63 such that warming events are primarily driven by changes in winter (Flückiger et al., 2008;
64 Zander et al., 2024), in the regional strength of the warming (Harrison and Sánchez Goñi, 2010)
65 and how warming relates to changes in moisture (Wei et al., 2021), there is a need for more
66 systematic reconstruction of seasonal climate changes.

67 In the paper, we provide reconstructions of seasonal temperature changes and changes in plant-
68 available moisture during the intervals corresponding to D-O warming events in Greenland
69 during Marine Isotope Stage 3 based on available pollen records globally. We employ a
70 standard methodology to construct age models for these records, as well as a standard
71 regression-based approach to make the reconstructions. We analyse the regional patterns to
72 identify key targets for model evaluation.

73 **2. Methods**

74 **2.1. Data sources**

75 Modern pollen data were obtained from version 2 of the SPECIAL Modern Pollen Data Set
76 (SMPDSv2: Villegas-Diaz and Harrison, 2022). This global data set contains 24649 modern
77 pollen records from 17827 sites. The dataset contains relative abundance records for 4816
78 pollen taxa, created after removing taxa that are not climatically diagnostic (e.g. obligate
79 aquatics, carnivorous species, cultivated plants). The data set provides several levels of
80 taxonomic aggregation; here we use the most aggregated level, where woody species were
81 generally combined at genus level and herbaceous species at sub-family or family level unless
82 they were palynologically distinctive, occupied distinctive ecological niches and were
83 sufficiently geographically widespread. This "amalgamated" data set contains relative
84 abundance information for 1338 taxa. These samples were aggregated by longitude, latitude
85 and elevation in order to remove duplicates. Counts for *Quercus*, *Quercus* (deciduous) and
86 *Quercus* (evergreen) were combined because of inconsistent differentiation of *Quercus* pollen
87 in different regional records. Deciduous and evergreen oaks occupy different areas of climate
88 space, particularly in terms of seasonal moisture; specifically, evergreen oaks are typically
89 found in areas characterised by winter rainfall such as the Mediterranean. Nevertheless, since
90 there are other plant taxa that are similarly diagnostic of such regimes, the amalgamation of
91 *Quercus* (deciduous) and *Quercus* (evergreen) should not have a major effect on the robustness
92 of our climate reconstructions. Taxa that occurred in less than 10 samples in the training data
93 set were not used to make reconstructions because it is unlikely that the available samples

94 provided a reasonable estimate of the climate space occupied by these rare taxa (Liu et al.,
95 2020). After filtering, the data set contains information on 591 individual pollen taxa from
96 17547 sites (Figure 1).

97 The SMPDSv2 also provides climatic information at each pollen site, specifically the mean
98 temperature of the coldest month (MTCO), mean temperature of the warmest month (MTWA),
99 and a moisture index (α) calculated as the ratio of actual evapotranspiration to equilibrium
100 evapotranspiration. These bioclimate variables reflect mechanistically distinct controls on
101 plant growth.

102 The fossil pollen data were obtained from the Abrupt Climate Changes and Environmental
103 Responses (ACER) database (Sánchez Goñi et al., 2017), which includes 93 records from the
104 last glacial period (73-15 ka) with sufficient resolution and dating control to detect sub-
105 millennial scale variability. Here we focus on the 73 records covering most of Marine Isotope
106 Stage 3 (50-30 ka); 54 of these records are from terrestrial sites and 19 from marine sites
107 (Figure 1; Table 1). The fossil data were taxonomically harmonised to be consistent with the
108 SMPDSv2.

109 **2.2. Climate reconstruction method**

110 We used tolerance-weighted Weighted Averaging Partial Least Squares (*fx*TWA-PLS: Liu et
111 al., 2020; Liu et al., 2023) regression to model the relationships between taxon abundances and
112 individual climate variables in the SMPDSv2 modern training dataset and then applied these
113 relationships to reconstruct past climate using the fossil assemblages from the ACER database
114 (Figure 2). *fx*TWA-PLS reduces the tendency of regression methods to compress
115 reconstructions towards the centre of the sampled climate range by applying a sampling
116 frequency correction to reduce the influence of uneven sampling of climate space and
117 weighting the contribution of individual taxa according to their climate tolerances (Liu et al.,
118 2020). Version 2 of *fx*TWA-PLS (*fx*TWA-PLS2, Liu et al., 2023) uses P-splines smoothing to
119 derive the frequency correction and applies this correction both in estimating the climate
120 optima and tolerances, and in the regression itself, producing a further improvement in model
121 performance compared to version 1 (Liu et al., 2020).

122 We evaluated the *fx*TWA-PLS models by comparing the reconstructions with observations
123 using leave-out cross-validation, where one site at a time was randomly selected as a test site

124 and sites that are both geographically close (within 50 km horizontal distance from the site)
125 and climatically close (within 2% of the full range of each climate variable in the dataset) were
126 removed from the training set along with this test site, to prevent redundancy in the climate
127 information from inflating the cross-validation goodness of fit, following Liu et al. (2020). We
128 selected the last significant number of components (p -value ≤ 0.01) and assessed model
129 performance using the root mean square error of prediction (RMSEP). Compression was
130 assessed using linear regression of the leave-out cross-validated reconstructions on to the
131 climate variable. Reconstructions of MTCO, MTWA and α were made for every sample in
132 each fossil record. Sample specific errors were estimated via bootstrapping, as described in Liu
133 et al. (2020). We corrected for the effect of changes in atmospheric CO₂ on plant water-use
134 efficiency, and hence the reconstructions of α (Figure S1), following Prentice et al. (2022).
135 Appropriate values of CO₂ were taken from the WAIS Divide ice core record (Bauska et al.,
136 2021).

137 **2.3. Age modelling**

138 Although the ACER database provides age models for each pollen record, the resolution of the
139 individual records is variable (mean resolution 474 years) and these models are often
140 imperfectly aligned with the dating of D-O events as recorded in the Greenland ice core, and
141 which have been shown to have a globally synchronous imprint through analysis of speleothem
142 records (Adolphi et al., 2019; Corrick et al., 2020). To create a better alignment, we used
143 dynamic time warping (DTW: Belman and Kalaba, 1959; Burstyn et al., 2021) to adjust the
144 age scale for each individual record (Figure 2). Dynamic time warping optimises the similarity
145 between two sequences by stretching or compressing one sequence in the time dimension to
146 match the other. Here, we use simulated mean annual temperature (MAT) from a transient
147 simulation of the interval 50-30 ka made with the LOVECLIM model (Menviel et al., 2014)
148 as the reference sequence compared to MAT calculated as the average of MTCO and MTWA
149 from the individual pollen records. We used the mid-point between the start dates of each D-O
150 event (Wolff et al., 2010; converted into AICC2012 timescale) to sub-divide each ACER
151 record into discrete intervals and modified the time scale of the reconstructed mean annual
152 temperature series in each interval to match the reference sequence, having normalised both
153 sequences to remove the influence of differences in absolute values and the amplitude of
154 changes. The adjusted age model for each ACER record was then applied to the reconstructions
155 of MTCO, MTWA, and α from that record for subsequent analyses.

156 2.4. Assessment of regional climate changes during Greenland D-O warming events

157 The magnitude of climate change during the interval corresponding to each D-O warming event
 158 as registered in Greenland is calculated individually for each climate variable at each site. To
 159 avoid making an assumption about the sign of the climate change at a site, we used a third-
 160 order polynomial to fit the reconstructions during the interval from 300 years before to 600
 161 years after the official start date of each event (Wolff et al., 2010; converted into AICC2012
 162 timescale) to determine whether the change was positive or negative. We used the ages
 163 corresponding to the minimum and maximum in the fitted polynomial ($t_{\min \text{ polynomial}}$, $t_{\max \text{ polynomial}}$).
 164 However, since the smoothed polynomial may underestimate or overestimate the
 165 amplitude of change, we used the reconstructed minimum or maximum value within the period
 166 $t_{\min \text{ polynomial}} \pm 100$ years or $t_{\max \text{ polynomial}} \pm 100$ years respectively (see Figure S2).

167 In cases where no change was registered for all of the three climate variables, we assume that
 168 the event was not registered at the site. As a measure of the accuracy of the DTW method to
 169 identify D-O events, we compared the number of identified events with the number of D-O
 170 events that occurred during the time covered by each record (Table 1). To assess whether events
 171 were missed in a particular record due to low sampling resolution, we examined the number of
 172 samples present in the 900-year interval covering the sampled D-O (i.e. 300 years before to
 173 600 years after the official start date of each event), where low resolution was defined as ≤ 3
 174 samples in this 900-year interval. Reconstructions covering intervals where a signal was not
 175 identified were not used in subsequent analyses.

176 We calculated sample-specific errors for the minimum and maximum reconstructed values.
 177 Assuming that the minimum and maximum values are independent, we used error propagation
 178 to obtain the error of the change:

$$179 \quad \sigma_{\text{change}} = \sqrt{\sigma_{\min}^2 + \sigma_{\max}^2}$$

180 Following Liu et al. (2022), we used a maximum likelihood method to estimate the ratio of
 181 ΔMTCO to ΔMTWA (and ratio of $\Delta\alpha$ to ΔMTWA) to take account of the errors on both
 182 variables.

183 3. Results

184 fx TWA-PLS reproduces the modern climate reasonably well (Table 2). The performance is
185 best for MTCO (R^2 0.75, RMSEP 6.51, slope 0.85) but is also good for MTWA (R^2 0.59,
186 RMSEP 3.68, slope 0.71) and α (R^2 0.65, RMSEP 0.18, slope 0.71). Assessment of the variance
187 inflation factor scores shows that there is no problem of multicollinearity so that it is possible
188 to reconstruct all three climate variables independently (Liu et al., 2023).

189 The use of dynamic time-warping made it possible to identify D-O events robustly (Table 1;
190 Supplementary Table 1). Thirteen of the 73 sites cover some part of the 50-30 ka periods but
191 do not include D-O events. Across the remaining 60 sites, we identified 278 out of the 348
192 individual D-O events (80%) that occurred during the intervals covered by the records. In the
193 majority of cases where a D-O event should have been registered but could not be identified in
194 an individual record (60 out of 70 cases), the resolution of that part of the record was extremely
195 poor (≤ 3 samples in the 900-year interval starting 300 years before to 600 years after the
196 official start date of the event).

197 Changes in both MTCO and MTWA were generally largest in the extratropics and were more
198 muted in the tropics (Figure 3). The change in MTCO was significantly larger in the northern
199 extratropics when considered across all D-O events and sites; the change in MTCO was larger,
200 but not significantly larger, in the southern extratropics; the changes in MTCO are not
201 correlated with the changes in MTWA in the tropics (Table 3). There is a significant positive
202 relationship between the change in α and the change in MTWA in all regions (Figure 4; Table
203 4).

204 The spatial patterns of changes in MTCO and MTWA show consistent features across multiple
205 D-O events (Figure 5), most noticeably that the largest warming occurs in the extratropics of
206 Eurasia, while western North America and the southern extratropics are characterised by
207 cooling. The anti-phasing between the northern and southern extratropics is consistent across
208 D-O events. Nevertheless, both the magnitude of the changes and the spatial patterns vary
209 between the D-O events (Figure S3; Figure S4). Changes in α broadly follow the changes in
210 temperature, with increased α in regions characterised by warming (Figure 5) but show more
211 variability both spatially and between D-O events (Figure S5). This is particularly true for
212 Europe, which is characterised by a mixed signal of drying and wetting.

213 4. Discussion and Conclusions

214 We have presented a first attempt to map the spatial patterns of quantitative changes in seasonal
215 temperature and plant-available moisture during D-O events globally, using a consistent
216 methodology and a single data source. These analyses show that there is an anti-phasing
217 between changes in the northern extratropics and the southern extratropics, with warming in
218 the north and cooling in the south. The largest and most consistent warming during D-O events
219 occurs in Eurasia. There is a significant difference in the warming during winter and summer
220 in the northern extratropics, resulting in an overall reduction in seasonality, but no significant
221 difference in the tropics and southern extratropics. Site-based reconstructions (e.g. Denton et
222 al., 2022; Zander et al., 2024) suggest much larger cooling in winter than summer during cold
223 phases of the last glacial, implying enhanced seasonality compared to warm intervals, which
224 would be consistent with our reconstructions of a reduction in seasonality during warming
225 events in the northern extratropics. Globally, there is a positive relationship between the change
226 in temperature and plant available moisture, as indicated by α . This is consistent with more
227 qualitative interpretation of palaeo-records from specific regions, where many regions are
228 characterised by both warming and wetting (e.g. western Europe: Sánchez Goñi et al., 2008;
229 Fletcher et al., 2010; eastern Europe: Fleitmann et al., 2009; Stockehecke et al., 2016; central
230 Siberia: Grygar et al., 2006; the Great Basin USA: Denniston et al., 2007; Jiménez-Moreno et
231 al., 2010). However, according to our reconstructions, the nature of this relationship varies
232 between regions: there are some regions that are characterised by warming and wetting, others
233 are characterised by warming and drying. Previous studies have also indicated drier conditions
234 during D-O events, particularly in parts of the USA such as the Pacific Northwest (Grigg and
235 Whitlock, 2002) and Florida (Grimm et al., 2006; Jiménez-Moreno et al., 2010) Although there
236 is some consistency in the broadscale patterns of changes across D-O events, the magnitude of
237 the changes as well as the spatial patterning varies between events.

238 We have used a global pollen data set for calibration of the pollen-climate relationships,
239 SMPDsv2 (Villegas-Diaz and Harrison, 2022). The use of a global data set, rather than region-
240 specific training data, relies on the principle of phylogenetic niche conservatism (Harvey and
241 Pagel, 1991), which states that traits tend to remain constant over time. This also applies to the
242 climate niche (Wiens and Graham, 2005; Wiens et al., 2010; Peterson, 2011; Crisp and Cook,
243 2012; Jiang et al., 2023) as evidenced by disjunct distributions of taxa across different
244 continents (Yin et al., 2021). Niche conservatism underpins the fact that the modern

245 distribution of specific genera can be predicted using climate-pollen relationships developed
246 from other regions (e.g. Huntley et al., 1989). The use of a global data set for calibration makes
247 it possible to sample a large range of climates, and thus makes it more likely that the
248 reconstructions of glacial climates are realistic and not confined to the limited climate range
249 sampled in any one region (Turner et al., 2020). Indeed, Turner et al. (2020) have shown that
250 increasing the size of the calibration data set tends to lead to smaller reconstruction errors and
251 more accurate estimates of taxon coefficients. Pragmatically, the use of a global data set also
252 facilitates making reconstructions for sites from regions where there is limited modern pollen
253 data.

254 These reconstructions can be used as targets for model evaluation, specifically the two transient
255 D-O experiments planned for the next phase of the Palaeoclimate Modelling Intercomparison
256 (see Malmierca-Vallet et al., 2023 for the experimental protocol). The first of these experiments
257 is a baseline simulation starting at 34 ka, a time with low obliquity, moderate MIS3 greenhouse
258 gas values, and an intermediate ice sheet configuration, which appears to be most conducive to
259 generating D-O-like behaviour in climate models. The second experiment involves the
260 addition of freshwater, to examine whether this is necessary to precondition a state conducive
261 to generating D-O events. The observed anti-phasing in temperature changes between the
262 northern and southern hemispheres is a general feature of climate model experiments. Most
263 models show larger warming in winter than in summer in the northern hemisphere (e.g.
264 Flückiger et al., 2008; Van Meersbeeck et al., 2011; Izumi et al., 2023), which is also consistent
265 with our reconstructions. Models generally show an intensification of the northern hemisphere
266 monsoons during D-O events (e.g. Menviel et al., 2020; Izumi et al., 2023), but there is less
267 consistency about changes in plant-available moisture in the extratropics. Our reconstructions
268 of α suggest an intensification of the northern hemisphere monsoons, consistent with the
269 simulations, and provide an opportunity to evaluate spatial patterns of moisture changes over
270 the extratropics. The reconstructions also indicate an increase in α across much of the tropics,
271 including northern South America, West Africa and southern China and Japan. Although α is
272 not a direct reflection of summer precipitation, these changes are consistent with enhanced
273 northern hemisphere monsoons during warming events, as shown by speleothem records from
274 the Caribbean (Warken et al., 2019) and speleothem and pollen records from Asia (Wang et al.,
275 2001; Zorzi et al., 2022; Fohlmeister et al., 2023). Although there is some consistency in the
276 broadscale patterns of changes in temperature and moisture across D-O events, the magnitude
277 of the changes as well as the spatial patterning varies between events.

278 Identifying D-O events in pollen records is often problematic, particularly in regions where
279 warming (especially if accompanied by dryer conditions) leads to a reduction (or an hiatus) in
280 sedimentation as reflected in the variable resolution of the available pollen records (e.g.
281 Sinopoli et al., 2019; Wei et al., 2021; Camuera et al., 2022; Pini et al., 2022). The use of shorter
282 periods (Alshehri et al., 2019) goes some way to improving the identification of potential D-O
283 events using dynamic time warping (Alshehri et al., 2019). Thus, we were able to identify D-
284 O events only 80% of the 348 individual D-O events that occurred during the intervals covered
285 by the 60 records available globally. It is also likely that some of the variability in the
286 reconstructed changes between different D-O events reflects imperfect identification of
287 specific events because of the comparatively modest resolution of the records. Several new
288 high-resolution records covering MIS3 have become available since the compilation of the
289 ACER database (e.g. Bird et al., 2024; Wei et al., 2021; Camuera et al., 2022; Pini et al., 2022;
290 Rowe et al., 2024; Shichi et al., 2023; Zorzi et al., 2022) and including these newer records
291 could help to improve the reliability of the global reconstructions presented here. Nevertheless,
292 this first compilation of quantitative climate reconstructions through multiple D-O events
293 during MIS3 provides an opportunity for evaluation of the transient D-O simulations planned
294 as part of the next phase of the Palaeoclimate Modelling Intercomparison Project (Malmierca-
295 Vallet et al., 2023).

296

297 **Data and code availability.** All the data used are public access and cited here. The code used
298 to generate the reconstructions and figures is available at [https://github.com/ml4418/DO-](https://github.com/ml4418/DO-climate-reconstruction-paper.git)
299 [climate-reconstruction-paper.git](https://github.com/ml4418/DO-climate-reconstruction-paper.git)

300 **Author contributions.** ML, SPH and ICP designed the study. ML made the reconstructions
301 and produced the figures and tables. ML and SPH carried out the analyses. SPH wrote the first
302 draft of the paper and all authors contributed to the final draft.

303 **Competing Interests.** The authors declare not competing interests.

304 **Acknowledgements.** ML acknowledges support from Imperial College through the Lee
305 Family Scholarship. ICP acknowledges support from the ERC under the European Union
306 Horizon 2020 research and innovation programme (grant agreement no.: 787203 REALM).
307 SPH acknowledges fruitful discussions with colleagues from the D-O community working
308 group.

309

310 **References**

- 311 Adolphi, F., Bronk Ramsey, C., Erhardt, T., Edwards, R. L., Cheng, H., Turney, C. S. M.,
312 Cooper, A., Svensson, A., Rasmussen, S. O., Fischer, H., and Muscheler, R.:
313 Connecting the Greenland ice-core and U / Th timescales via cosmogenic
314 radionuclides: testing the synchronicity of Dansgaard–Oeschger events, *Clim. Past*, 14,
315 1755–1781, <https://doi.org/10.5194/cp-14-1755-2018>, 2018.
- 316 Alshehri, M., Coenen, F., and Dures, K.: Effective sub-sequence-based dynamic time warping.
317 In: Bramer, M., Petridis, M. (eds) *Artificial Intelligence XXXVI. SGAI 2019. Lecture*
318 *Notes in Computer Science*, 11927. Springer, Cham. [https://doi.org/10.1007/978-3-](https://doi.org/10.1007/978-3-030-34885-4_23)
319 [030-34885-4_23](https://doi.org/10.1007/978-3-030-34885-4_23), 2019.
- 320 Ampel, L., Bigler, C., Wohlfarth, B., Risberg, J., Lotter, A.F., and Veres, D.: Modest summer
321 temperature variability during DO cycles in western Europe, *Quat. Sci. Rev.*, 29, 1322–
322 1327, <https://doi.org/10.1016/j.quascirev.2010.03.002>, 2010.
- 323 Bauska, T. K., Marcott, S. A. and Brook, E. J.: Abrupt changes in the global carbon cycle
324 during the last glacial period, *Nat. Geosci.*, 14(2), 91–96, doi:10.1038/s41561-020-
325 00680-2, 2021.
- 326 Bellman, R., and Kalaba, R.: On adaptive control processes, *Automatic Control, IRE*
327 *Transactions*, 4, 1–9, http://ieeexplore.ieee.org/xpls/abs_all.jsp?arnumber=1104847,
328 1959.
- 329 Bird, M., Brand, M., Comley, R., Fu, X., Hadeen, X., Jacobs, Z., Rowe, C., Wurster, C., Zwart,
330 C. and Bradshaw, C.: Late Pleistocene emergence of an anthropogenic fire regime in
331 Australia’s tropical savannahs, *Nat. Geosci.*, 17, doi:10.1038/s41561-024-01388-3,
332 2024.
- 333 Burstyn, Y., Gazit, A., and Omri Dvir, O.: Hierarchical Dynamic Time Warping methodology
334 for aggregating multiple geological time series, *Comp. & Geosci.*, 150, 104704,
335 <https://doi.org/10.1016/j.cageo.2021.104704>, 2021.

- 336 Camuera, J., Ramos-Román, M.J., Jiménez-Moreno, G. *et al.*: Past 200 kyr hydroclimate
337 variability in the western Mediterranean and its connection to the African Humid
338 Periods, *Sci. Rep.*, 12, 9050, <https://doi.org/10.1038/s41598-022-12047-1>, 2022.
- 339 Corrick, E.C., Drysdale, R.N., Hellstrom, J.C., Capron, E., Rasmussen, S.O., Zhang, X.,
340 Fleitmann, D., Couchoud, I., and Wolff, E.: Synchronous timing of abrupt climate
341 changes during the last glacial period, *Science*, 369, 963–969,
342 <https://doi.org/10.1126/science.aay5538>, 2020.
- 343 Crisp, M. D. and Cook, L. G.: Phylogenetic niche conservatism: What are the underlying
344 evolutionary and ecological causes?, *New Phytol.*, 196(3), 681–694,
345 [doi:10.1111/j.1469-8137.2012.04298.x](https://doi.org/10.1111/j.1469-8137.2012.04298.x), 2012.
- 346 Dansgaard, W., Johnsen, S.J., Clausen, H.B., Dahl-Jensen, D., Gundestrup, N.S., Hammer,
347 C.U., Hvidberg, C.S., Steffensen, J.P., Sveinbjörnsdóttir, A.E., Jouzel, J., and Bond,
348 G.: Evidence for general instability of past climate from a 250-kyr ice-core record,
349 *Nature*, 364, 218–220, <https://doi.org/10.1038/364218a0>, 1993.
- 350 Denniston, R.F., Asmerom, Y., Polyak, V., Dorale, J.A., Carpenter, S.J., Trodick, C., Hoye,
351 B., and González, L.A.: Synchronous millennial-scale climatic changes in the Great
352 Basin and the North Atlantic during the last interglacial. *Geology* 35, 619–622, 2007.
- 353 Doblus-Reyes, F. J., Sörensson, A. A., Almazroui, M., Dosio, A., Gutowski, W. J., Haarsma,
354 R., Hamdi, R., Hewitson, B., Kwon, W.-T., Lamptey, B. L., Maraun, D., Stephenson,
355 T. S., Takayabu, I., Terray, L., Turner, A. and Zuo, Z.: Linking global to regional
356 climate change, in *Climate Change 2021 – The Physical Science Basis: Working Group*
357 *I Contribution to the Sixth Assessment Report of the Intergovernmental Panel on*
358 *Climate Change*, edited by V. Masson-Delmotte, P.Zhai, A. Pirani, S. L. Connors, C.
359 Péan, S. Berger, N. Caud, Y. Chen, L. Goldfarb, M. I. Gomis, M. Huang, K. Leitzell,
360 E.Lonnoy, J. B. R. Matthews, T. K. Maycock, T. Waterfield, O. Yelekçi, R. Yu, and B.
361 Zhou, pp. 1363–1512, Cambridge University Press, Cambridge, United Kingdom and
362 New York, NY, USA., 2021. Fleitmann, D., Cheng, H., Badertscher, S., Edwards, R.L.,
363 Mudelsee, M., Göktürk, O.M., Fankhauser, A., Pickering, R., Raible, C.C., Matter, A.,
364 Kramers, J., and Tüysüz, O.: Timing and climatic impact of Greenland interstadials
365 recorded in stalagmites from northern Turkey, *Geophys. Res. Lett.*, 36, 2009.

- 366 Fletcher, W.F., Sánchez Goñi, M.F., Allen, J.R.M., Cheddadi, R., Combourieu-Nebout, N.,
367 Huntley, B., Lawson, I., Londeix, L., Magri, D., Margari, V., Müller, U.C., Naughton,
368 F., Novenko, E., Roucoux, K., Tzedakis, P.C.: Millennial-scale variability during the
369 last glacial in vegetation records from Europe, *Quat. Sci. Rev.*, 29, 2839-2864,
370 <https://doi.org/10.1016/j.quascirev.2009.11.015>, 2010.
- 371 Flückiger, J., Knutti, R., White, J.W.C., and Renssen, H.: Modeled seasonality of glacial abrupt
372 climate events, *Clim. Dyn.*, 31, 633–645, <https://doi.org/10.1007/s00382-008-0373-y>,
373 2008.
- 374 Fohlmeister, J., Sekhon, N., Columbu, A., Vettoretti, G., Weitzel, N., Rehfeld, K., Veiga-Pires,
375 C., Ben-Yami, M., Marwan, N. and Boers, N.: Global reorganization of atmospheric
376 circulation during Dansgaard–Oeschger cycles, *Proc. Natl. Acad. Sci.*, 120(36),
377 e2302283120, doi:10.1073/pnas.2302283120, 2023.
- 378 Grigg, L.D., and Whitlock, C.: Patterns and causes of millennial-scale climate change in the
379 Pacific Northwest during Marine Isotope Stages 2 and 3, *Quat. Sci. Rev.*, 21, 2067-
380 2083, 2002.
- 381 Grimm, E.C., Watts, W.A., Jacobson, G.L., Hansen, B.C.S., Almquist, H., and Dieffenbacher-
382 Krall, A.C.: Evidence for warm wet Heinrich events in Florida, *Quat. Sci. Rev.*, 25,
383 2197-2211, 2006.
- 384 Grygar, T., Kadlec, J., Pruner, P., Swann, G., Bezdicka, P., Hradil, D., Lang, K., Novotna, K.,
385 and Oberhänsli, H.: Paleoenvironmental record in Lake Baikal sediments:
386 environmental changes in the last 160 ky, *Palaeogeogr. Palaeoclimatol. Palaeoecol.*,
387 237, 240-254, 2006.
- 388 Guiot, J., de Beaulieu, J. L., Cheddadi, R., David, F., Ponel, P., and Reille, M.: The climate in
389 Western Europe during the last Glacial/Interglacial cycle derived from pollen and insect
390 remains, *Palaeogeogr., Palaeoclimatol., Palaeoecol.*, 103, 73–93,
391 [https://doi.org/10.1016/0031-0182\(93\)90053-L](https://doi.org/10.1016/0031-0182(93)90053-L), 1993.
- 392 Jiménez-Moreno, G., Anderson, R.S., Desprat, S., Grigg, L.D., Grimm, E.C., Heusser, L.E.,
393 Jacobs, B.F., López-Martínez, C., Whitlock, C.L., and Willard, D.A.: Millennial-scale

- 394 variability during the last glacial in vegetation records from North America, *Quat. Sci.*
395 *Rev.*, 29, 2865-2881, <https://doi.org/10.1016/j.quascirev.2009.12.013>, 2010.
- 396 Harrison, S.P., and Sánchez Goñi, M.F.: Global patterns of vegetation response to millennial-
397 scale variability during the last glacial: A synthesis. *Quat. Sci. Rev.*, 29, 2957-2980,
398 2010.
- 399 Harvey, P. H. and Pagel, M. D.: *The comparative method in evolutionary biology*, Oxford
400 University Press., 1991.
- 401 Huber, C., Leuenberger, M., Spahni, R., Flückiger, J., Schwander, J., Stocker, T.F., Johnsen,
402 S., Landais, A., and Jouzel, J.: Isotope calibrated Greenland temperature record over
403 Marine Iso- tope Stage 3 and its relation to CH₄, *Earth Planet. Sci. Lett.*, 243, 504–519,
404 2006.
- 405 Huntley, B., Bartlein, P. J. and Prentice, I. C.: Climatic control of the distribution and
406 abundance of Beech (*Fagus L.*) in Europe and North America, *J. Biogeogr.*, 16(6), 551–
407 560, doi:10.2307/2845210, 1989.
- 408 Huntley, B., Watts, W.A., Allen, J.R.M., Zolitschka, B.: Palaeoclimate, chronology and
409 vegetation history of the Weichselian Lateglacial: comparative analysis of data from
410 three cores at Lago Grande di Monticchio, southern Italy, *Quat. Sci. Rev.*, 18: 945-960,
411 [https://doi.org/10.1016/S0277-3791\(99\)00007-4](https://doi.org/10.1016/S0277-3791(99)00007-4), 1999.
- 412 IPCC: *Climate change 2022: Impacts, adaptation and vulnerability. Contribution of working*
413 *group II to the sixth assessment report of the Intergovernmental Panel on Climate*
414 *Change*, edited by H.-O. Pörtner, D. C. Roberts, M. Tignor, E. S. Poloczanska, K.
415 Mintenbeck, A. Alegría, M. Craig, S. Langsdorf, S. Löschke, V. Möller, A. Okem, and
416 B. Rama, Cambridge University Press, Cambridge University Press, Cambridge, UK
417 and New York, NY, USA., 2022.
- 418 Jiang, K., Wang, Q., Dimitrov, D., Luo, A., Xu, X., Su, X., Liu, Y., Li, Y., Li, Y. and Wang, Z.:
419 Evolutionary history and global angiosperm species richness–climate relationships,
420 *Glob. Ecol. Biogeogr.*, 32(7), 1059–1072, doi:10.1111/geb.13687, 2023.

- 421 Kindler, P., Guillevic, M., Baumgartner, M., Schwander, J., Landais, A., and Leuenberger, M.:
422 Temperature reconstruction from 10 to 120 kyr b2k from the NGRIP ice core, *Clim.*
423 *Past*, 10, 887–902, <https://doi.org/10.5194/cp-10-887-2014>, 2014.
- 424 Lee, J.-Y., Marotzke, J., Bala, G., Cao, L., Corti, S., Dunne, J. P., Engelbrecht, F., Fischer, E.,
425 Fyfe, J. C., Jones, C., Maycock, A., Mutemi, J., Ndiaye, O., Panickal, S. and Zhou, T.:
426 Future global climate: Scenario-based projections and near-term information, in
427 *Climate change 2021: The physical science basis. Contribution of working group I to*
428 *the sixth assessment report of the Intergovernmental Panel on Climate Change*, edited
429 by V. Masson-Delmotte, P. Zhai, A. Pirani, S. L. Connors, C. Péan, S. Berger, N. Caud,
430 Y. Chen, L. Goldfarb, M. I. Gomis, M. Huang, K. Leitzell, E. Lonnoy, J. B. R.
431 Matthews, T. K. Maycock, T. Waterfield, O. Yelekçi, R. Yu, and B. Zhou, pp. 553–672,
432 Cambridge University Press, Cambridge, United Kingdom and New York, NY, USA.,
433 2021.
- 434 Liu, M., Prentice, I.C., ter Braak, C.J.F, and Harrison, S.P.: An improved statistical approach
435 for reconstructing past climates from biotic assemblages, *Proc. Royal Soc., Math. A*,
436 476, 20200346, 20200346, <https://doi.org/10.1098/rspa.2020.0346>, 2020.
- 437 Liu, M., Shen, Y., González-Sampéris, P., Gil-Romera, G., ter Braak, C.J.F. Prentice, I.C., and
438 Harrison, S.P.: Holocene climates of the Iberian Peninsula, *Clim. Past* 19, 803-834,
439 <https://doi.org/10.5194/cp-19-803-2023>, 2023.
- 440 Malmierca-Vallet, I., Sime, L.C., and the D–O community members: Dansgaard–Oeschger
441 events in climate models: review and baseline Marine Isotope Stage 3 (MIS3) protocol,
442 *Clim. Past*, 19, 915–942, <https://doi.org/10.5194/cp-19-915-2023>, 2023.
- 443 Menviel, L., Timmermann, A., Friedrich, T., and England, M. H.: Hindcasting the continuum
444 of Dansgaard–Oeschger variability: mechanisms, patterns and timing, *Clim. Past* 10,
445 63–77, 2014.
- 446 Menviel, L.C., Skinner, L.C., Tarasov, L., and Tzedakis, P.C.: An ice–climate oscillatory
447 framework for Dansgaard–Oeschger cycles, *Nat. Rev. Earth Environ.*, 1, 677–693,
448 <https://doi.org/10.1038/s43017-020-00106-y>, 2020.

- 449 Peterson, A. T.: Ecological niche conservatism: A time-structured review of evidence, *J.*
450 *Biogeogr.*, 38(5), 817–827, doi:10.1111/j.1365-2699.2010.02456.x, 2011.
- 451 Pini, R., Furlanetto, G., Vallé, F., Badino, F., Wick, L., Anselmetti, F.S., Bertuletti, P., Fusi, N.,
452 Morlock, M.A., Delmonte, B., Harrison, S.P., Maggi, V., Ravazzi, C.: Linking North
453 Atlantic and Alpine Last Glacial Maximum climates via a high-resolution pollen-based
454 subarctic forest steppe record, *Quat. Sci. Rev.*, 294, 107759,
455 <https://doi.org/10.1016/j.quascirev.2022.107759>, 2022.
- 456 Prentice, I. C., Villegas-Diaz, R. and Harrison, S. P.: Accounting for atmospheric carbon
457 dioxide variations in pollen-based reconstruction of past hydroclimates, *Glob. Planet.*
458 *Change*, 211, 103790, doi:10.1016/j.gloplacha.2022.103790, 2022.
- 459 Prud'homme, C., Fischer, P., Jöris, O., Gromov, S., Vinnepand, M., Hatté, C., Vonhof, H.,
460 Moine, O., Vött, A., and Fitzsimmons, K. E.: Millennial-timescale quantitative
461 estimates of climate dynamics in central Europe from earthworm calcite granules in
462 loess deposits, *Commun. Earth Environ.*, 3, 1–14, [https://doi.org/10.1038/s43247-022-](https://doi.org/10.1038/s43247-022-00595-3)
463 [00595-3](https://doi.org/10.1038/s43247-022-00595-3), 2022.
- 464 Rowe, C., Brand, M., Wurster, C. M. and Bird, M. I.: Vegetation changes through stadial and
465 interstadial stages of MIS 4 and MIS 3 based on a palynological analysis of the
466 Girraween Lagoon sediments of Darwin, Australia, *Palaeogeogr. Palaeoclimatol.*
467 *Palaeoecol.*, 642, 112150, doi:10.1016/j.palaeo.2024.112150, 2024.
- 468 Sánchez Goñi, M., Cacho, I., Turon, J., Guiot, J., Sierro, F., Peyrouquet, J., Grimalt, J. and
469 Shackleton, N.: Synchronicity between marine and terrestrial responses to millennial
470 scale climatic variability during the last glacial period in the Mediterranean region,
471 *Clim. Dyn.*, 19(1), 95–105, doi:10.1007/s00382-001-0212-x, 2002.
- 472 Sánchez Goñi, M.F., and Harrison, S.P.: Millennial-scale climate variability and vegetation
473 changes during the Last Glacial: Concepts and terminology, *Quat. Sci. Rev.*, 29, 2823–
474 2827, 2010.
- 475 Sánchez Goñi, M.F., Desprat, S., Daniau, A.-L., Bassinot, F., Polanco-Martínez, J.M., Harrison,
476 S.P., Allen, J.R.P., Anderson, R.S., Behling, H., Bonnefille, R., Burjachs, F., Carrión,
477 J.S., Cheddadi, R., Clark, J.S., Combourieu-Nebout, N., Courtney-Mustaphi, C.,

- 478 Debusk, G.H., Dupont, L.M., Finch, J., Fletcher, W.J., Giardini, M., González, C.,
479 Gosling, W.D., Grigg, L.D., Grimm, E.C., Hayashi, R., Helmens, K., Heusser, L.E.,
480 Hill, T., Hope, G., Huntley, B., Igarashi, Y., Irino, T., Jacobs, B.F., Jiménez-Moreno, G.,
481 Kawai, S., Kershaw, P., Kumon, F., Lawson, I., Ledru, M.-P., Lézine, A.-M., Liew, P.-
482 M., Magri, D., Marchant, R., Margari, V., Mayle, F., McKenzie, M., Moss, P., Müller,
483 S., Müller, U.C., Naughton, F., Newnham, R.M., Oba, T., Pérez-Obiol, R., Pini, R.,
484 Ravazzi, C., Roucoux, K.H., Rucina, S., Scott, L., Takahara, H., Tzedakis, P.C., Urrego,
485 D.H., Van Geel, B., Valencia, B.G., Vandergoes, M.J., Vincens, A., Whitlock, C.L.,
486 Willard, D. A., and Yamamoto, M.: The ACER pollen and charcoal database: a global
487 resource to document vegetation and fire response to abrupt climate changes of the last
488 glacial period, *Earth Syst. Sci. Data* 9: 679-695, 2017.
- 489 Shichi, K., Goebel, T., Izuho, M. and Kashiwaya, K.: Climate amelioration, abrupt vegetation
490 recovery, and the dispersal of *Homo sapiens* in Baikal Siberia, *Sci. Adv.*, 9(38),
491 eadi0189, doi:10.1126/sciadv.adi0189, 2024.
- 492 Sinopoli, G., Peyron, O., Masi, A., Holtvoeth, J., Francke, A., Wagner, B., and Sadori, L.:
493 Pollen-based temperature and precipitation changes in the Ohrid Basin (western
494 Balkans) between 160 and 70 ka, *Clim. Past*, 15, 53–71, [https://doi.org/10.5194/cp-15-](https://doi.org/10.5194/cp-15-53-2019)
495 53-2019, 2019.
- 496 Stockhecke, M., Timmermann, A., Kipfer, R., Haug, G.H., Kwiecien, O., Friedrich, T.,
497 Meniel, L., Litt, T., Pickarski, N., and Anselmetti, F.S.: Millennial to orbital-scale
498 variations of drought intensity in the Eastern Mediterranean, *Quat. Sci. Rev.*, 133, 77-
499 95, 2016.
- 500 Turner, M. G., Wei, D., Prentice, I. C. and Harrison, S. P.: The impact of methodological
501 decisions on climate reconstructions using WA-PLS, *Quat. Res.*, 99, 341–356,
502 doi:10.1017/qua.2020.44, 2021.
- 503 Újvári, G., Bernasconi, S. M., Stevens, T., Kele, S., Páll-Gergely, B., Surányi, G., and Demény,
504 A.: Stadial-Interstadial Temperature and Aridity Variations in East Central Europe
505 Preceding the Last Glacial Maximum, *Paleoceanog. Paleoclim.*, 36, e2020PA004170,
506 <https://doi.org/10.1029/2020PA004170>, 2021.

- 507 Van Meerbeeck, C.J., Renssen, H., Roche, D.M., Wohlfarth, B., Bohncke, S.J.P., Bos, J.A.A.,
508 Engels, S., Helmens, K.F., Sánchez-Goñi, M.F., Svensson, A., and Vandenberghe, J.:
509 The nature of MIS 3 stadial-interstadial transitions in Europe: New insights from
510 model-data comparisons, *Quat. Sci. Rev.*, 30, 3618–3637,
511 <https://doi.org/10.1016/j.quascirev.2011.08.002>, 2011.
- 512 Villegas-Diaz, R., and Harrison, S.P.: The SPECIAL Modern Pollen Data Set for Climate
513 Reconstructions, version 2 (SMPDSv2). University of Reading.
514 Dataset. <https://doi.org/10.17864/1947.000389>, 2022.
- 515 Voelker, A.H.: Global distribution of centennial-scale records for Marine Isotope Stage (MIS)
516 3: a database, *Quat. Sci. Rev.*, 21, 1185–1212, 2002.
- 517 Wang, Y. J., Cheng, H., Edwards, R. L., An, Z. S., Wu, J. Y., Shen, C.-C. and Dorale, J. A.: A
518 high-resolution absolute-dated Late Pleistocene monsoon record from Hulu Cave,
519 China, *Science* (80-.), 294(5550), 2345–2348, doi:10.1126/science.1064618, 2001.
- 520 Warken, S. F., Scholz, D., Spötl, C., Jochum, K. P., Pajón, J. M., Bahr, A. and Mangini, A.:
521 Caribbean hydroclimate and vegetation history across the last glacial period, *Quat. Sci.*
522 *Rev.*, 218, 75–90, doi:10.1016/j.quascirev.2019.06.019, 2019.
- 523 Wei, D., González-Sampériz, P., Gil-Romera, G., Harrison, S.P., and Prentice, I.C.: Seasonal
524 temperature and moisture changes in interior semi-arid Spain from the last interglacial
525 to the Late Holocene, *Quat. Res.*, 101, 143–155, <https://doi.org/10.1017/qua.2020.108>,
526 2021.
- 527 Wiens, J. and Graham, C.: Niche conservatism: Integrating evolution, ecology, and
528 conservation biology, *Annu. Rev. Ecol. Evol. Syst.*, 36, 519–539,
529 doi:10.1146/annurev.ecolsys.36.102803.095431, 2005.
- 530 Wolff, E. W., Chappellaz, J., Blunier, T., Rasmussen, S. O. and Svensson, A.: Millennial-scale
531 variability during the last glacial: The ice core record, *Quat. Sci. Rev.*, 29(21), 2828–
532 2838, doi:10.1016/j.quascirev.2009.10.013, 2010.
- 533 Yin, X., Jarvie, S., Guo, W.-Y., Deng, T., Mao, L., Zhang, M., Chu, C., Qian, H., Svenning, J.-
534 C. and He, F.: Niche overlap and divergence times support niche conservatism in

535 eastern Asia–eastern North America disjunct plants, *Glob. Ecol. Biogeogr.*, 30(10),
536 1990–2003, doi:10.1111/geb.13360, 2021.

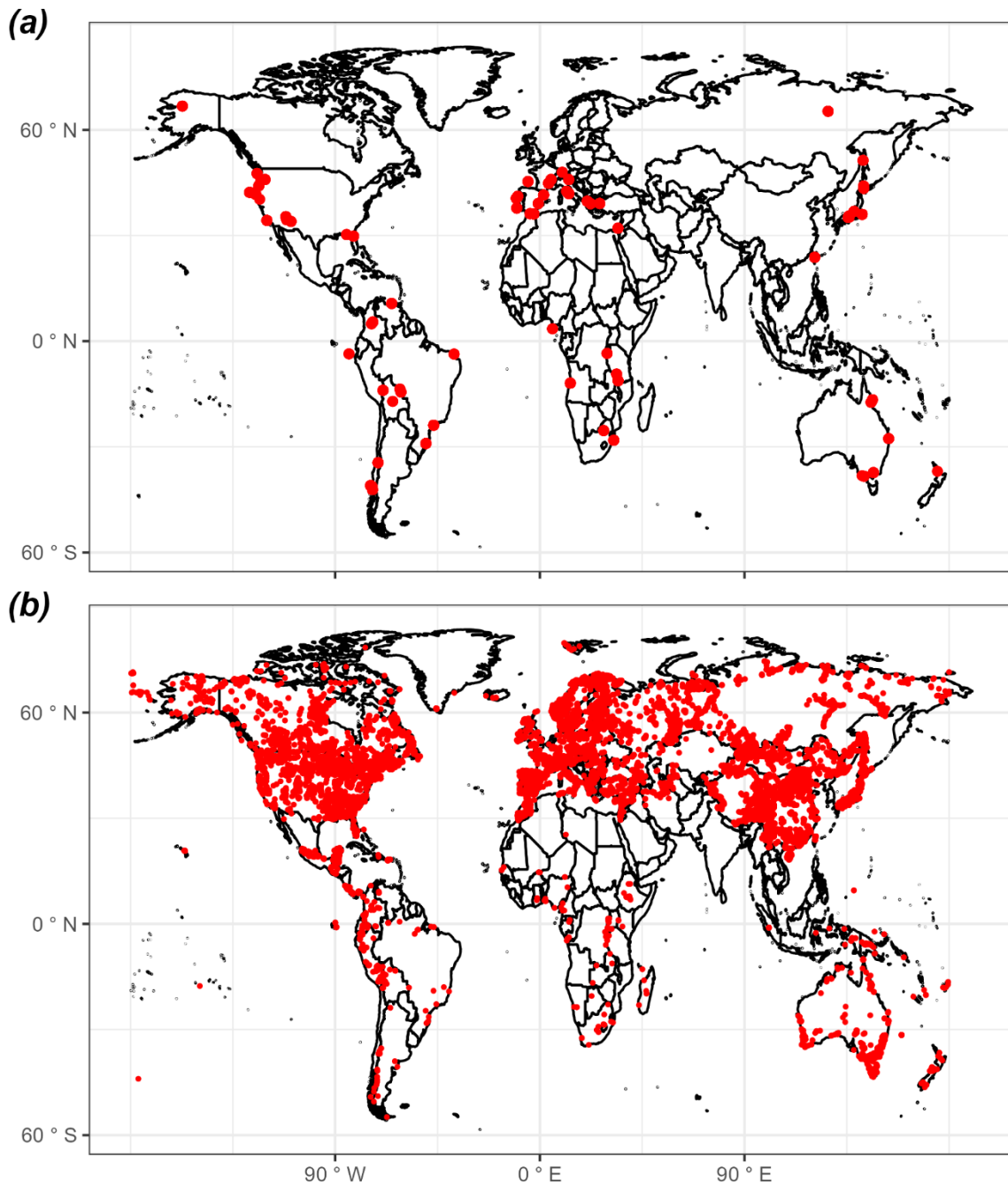
537 Zander, P. D., Böhl, D., Sirocko, F., Auderset, A., Haug, G. H. and Martínez-García, A.:
538 Reconstruction of warm-season temperatures in central Europe during the past 60 000
539 years from lacustrine branched glycerol dialkyl glycerol tetraethers (brGDGTs), *Clim.*
540 *Past*, 20(4), 841–864, doi:10.5194/cp-20-841-2024, 2024.

541 Zorzi, C., Desprat, S., Clément, C., Thirumalai, K., Oliviera, D., Anupama, K., Prasad, S. and
542 Martinez, P.: When eastern India oscillated between desert versus savannah-dominated
543 vegetation, *Geophys. Res. Lett.*, 49(16), e2022GL099417,
544 doi:10.1029/2022GL099417, 2022.

545

546 **Figures and Tables**

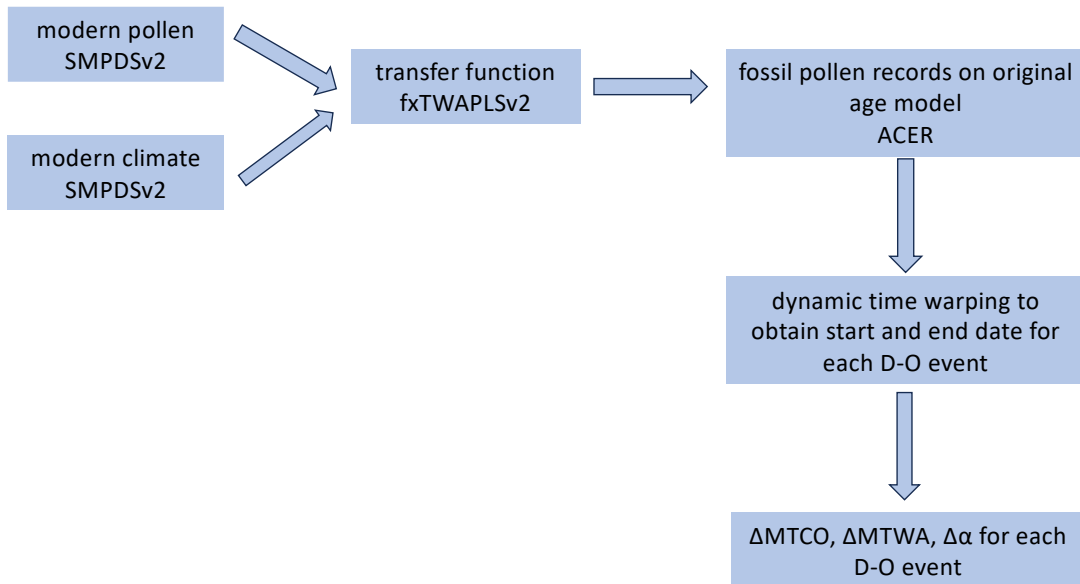
547 Figure 1: Map showing the locations of sites (a) from the Abrupt Climate Changes and
548 Environmental Responses (ACER) database (Sánchez Goñi et al., 2017) covering the interval
549 between 50 ka and 30 ka used for the reconstructions and (b) sites in version 2 of the SPECIAL
550 Modern Pollen Data Set (SMPDSv2: Villegas-Diaz and Harrison, 2022) used to derive the
551 transfer functions for these climate reconstructions.



552

553

554 Figure 2: Flow chart showing the reconstruction methodology.



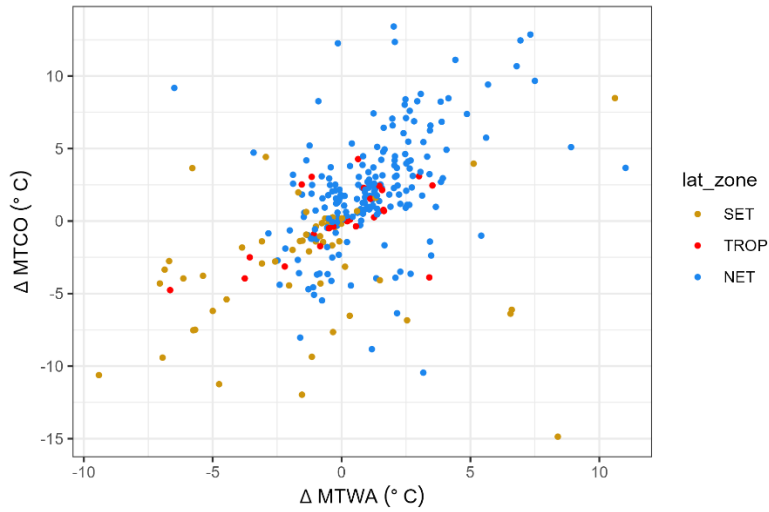
555

556

557

558

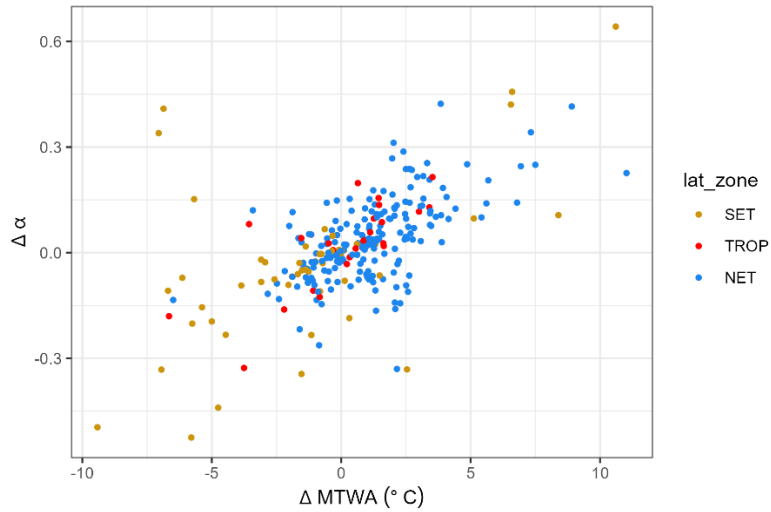
559 Figure 3: Scatter plot of the change in mean temperature of the coldest month (ΔMTCO) versus
560 the change in mean temperature of the warmest month (ΔMTWA) during individual
561 Dansgaard-Oeschger (D-O) events at individual sites. The points are colour-coded to indicate
562 whether the sites are from the northern extratropics (NET, north of 23.5°N), the tropics (TROP,
563 between 23.5°N and 23.5°S) or southern extratropics (SET, south of 23.5°S).



564

565

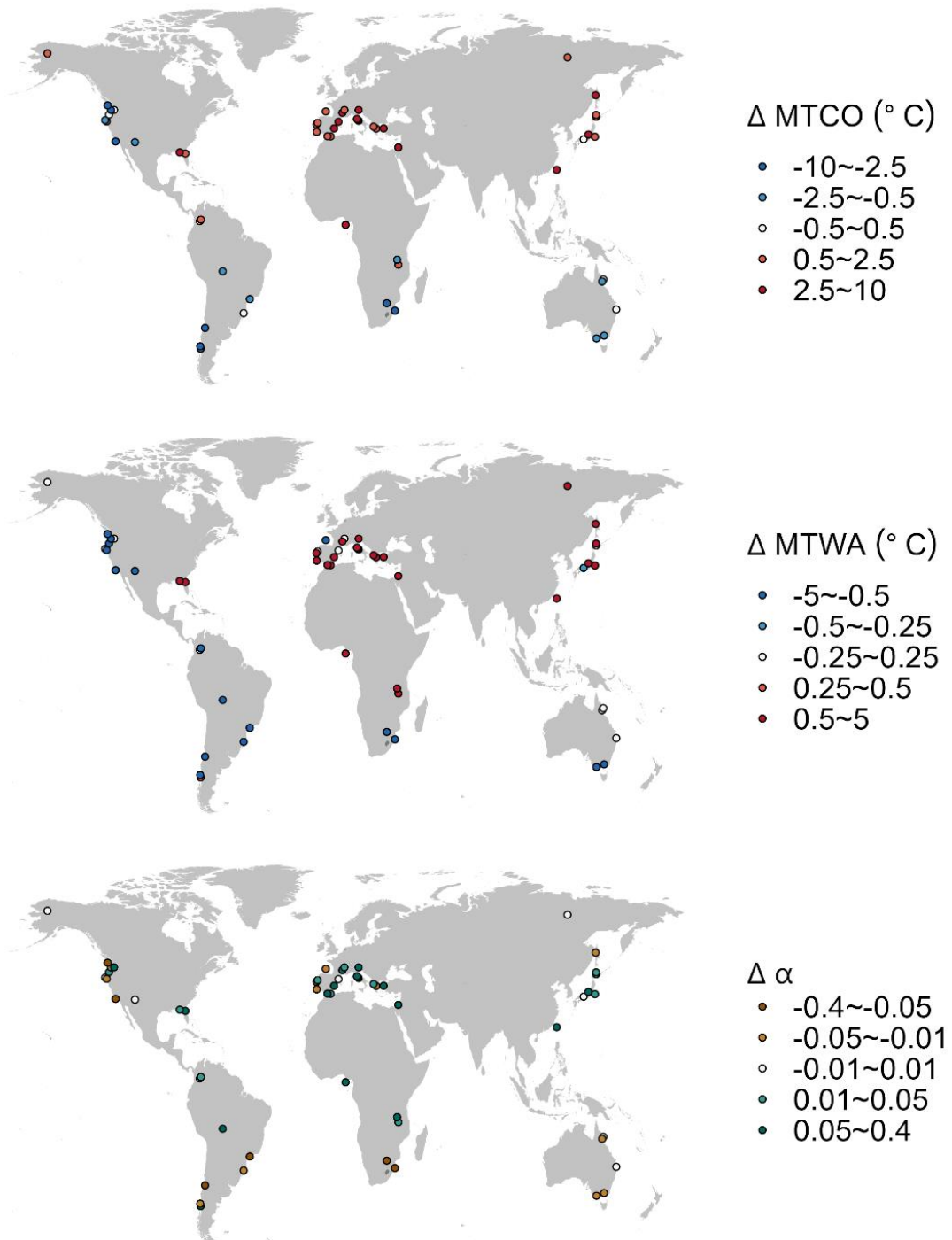
566 Figure 4: Scatter plot of the change in plant-available moisture ($\Delta\alpha$) versus the change in mean
567 temperature of the warmest month (ΔMTWA) during individual Dansgaard-Oeschger (D-O)
568 events at individual sites. The points are colour-coded to indicate whether the sites are from
569 the northern extratropics (NET, north of 23.5°N), the tropics (TROP, between 23.5°N and
570 23.5°S) or southern extratropics (SET, south of 23.5°S).



571

572

573 Figure 5: Maps showing the median change of site-based reconstructions for Dansgaard-
 574 Oeschger (D-O) events.



575

576

577 Table 1: Details of the sites from the Abrupt Climate Changes and Environmental Responses
 578 (ACER) database (Sánchez Goñi et al., 2017) covering the interval between 50 ka and 30 ka
 579 used for the climate reconstructions. n_{due} is the number of D-O events that should be found
 580 based on the time interval covered by the record. n_{miss} is the number of D-O events that were
 581 not identified. n_{low} is the number of D-O events missed because of low resolution of part of the
 582 record. Some of the 73 sites (indicated by / in n_{due} , n_{miss} and n_{low}) provide records for parts of
 583 the 50-30ka interval but not for the intervals of the D-O events. Reconstructions based on
 584 samples where the D-O signal was not identified were not used in subsequent analyses. The
 585 full citations for each site are given in Supplementary Information.

Site name	Latitude	Longitude	Elevation (m)	Site type	Reference(s)	n_{due}	n_{miss}	n_{low}
Abric Romani	41.53	1.68	350	TERR	Burjachs & Ramon (1994)	2	0	0
Azzano Decimo	45.8833	12.7165	10	TERR	Pini et al. (2009)	6	2	2
Caledonia Fen	-37.3333	146.7333	1280	TERR	Kershaw et al. (2007b)	8	2	2
Cambara do Sul	-29.05	-50.1	1040	TERR	Behling et al. (2004)	7	0	0
Camel Lake	30.26	-85.01	20	TERR	Watts et al. (1992)	2	1	1
Carp Lake	45.91	-120.88	720	TERR	Whitlock and Bartlein (1997); Whitlock et al. (2000)	8	1	1
Colônia	-23.87	-46.71	900	TERR	Ledru et al. (2009)	7	4	4
Core Trident 163 31B	-3.61	-83.96	-3210	MARI	Heusser and Shackleton (1994)	/	/	/
Fargher Lake	45.88	-122.58	200	TERR	Grigg and Whitlock (2002)	8	1	1
Fundo Nueva	-41.28	-73.83	66	TERR	Heusser et al. (2000)	6	1	0
Fuquene	5.45	-73.46	2540	TERR	van Geel and van der Hammen (1973); Mommersteeg (1998)	7	2	2
Füramoos	47.98	9.88	662	TERR	Müller et al. (2003)	/	/	/
GeoB3104	-3.67	-37.72	-767	MARI	Behling et al. (2000)	/	/	/
Hay Lake	34	-109.425	2780	TERR	Jacobs (1985)	5	4	4
Ioannina	39.75	20.85	470	TERR	Tzedakis et al. (2002); Tzedakis et al. (2004)	8	1	0
Joe Lake	66.76667	-157.217	183	TERR	Anderson (1988); Anderson et al. (1994)	7	3	3
Kalaloch	47.6053	-124.371	19	TERR	Heusser (1972)	8	2	0
Kamiyoshi Basin (KY01)	35.102	135.586	335	TERR	Takahara et al. (2000); Takahara et al. (2007); Hayashi et al. (2009)	1	0	0
Kashiru Bog	-3.47	29.57	2240	TERR	Bonnefille & Riollet (1988); Bonnefille et al. (1992)	2	2	2
Kenbuchi Basin	44.05	142.383	135	TERR	Igarashi et al. (1993); Igarashi (1996)	3	0	0
Khoe	51.341	142.14	15	TERR	Igarashi et al. (2002)	6	1	1
Kohuora	-36.95	174.8667	5	TERR	Newnham et al. (2007)	/	/	/
Kurota Lowland	35.517	135.879	20	TERR	Takahara & Kitagawa (2000)	/	/	/
KW31	3.52	5.57	-1181	MARI	Lézine & Cazet (2005);	2	0	0

					Lézine et al. (2005)			
La Laguna	4.92	-74.03	2900	TERR	Helmens et al., 1(1996)	2	0	0
Lac du Bouchet	44.83	3.82	1200	TERR	Reille and de Beaulieu (1990)	8	0	0
Lagaccione	42.57	11.8	355	TERR	Magri (1999); Magri (2008)	7	2	2
Laguna Bella Vista	-13.6167	-61.55	600	TERR	Burbridge et al. (2004)	2	1	1
Laguna Chaplin	-14.4667	-61.0667	600	TERR	Burbridge et al. (2004)	1	1	1
Lake Billyakh	65.2833	126.7833	340	TERR	Müller et al. (2010)	4	0	0
Lake Biwa (BIW95-4)	35.245	136.054	84	TERR	Takemura et al. (2000); Hayashida et al. (2007); Hayashi et al. (2010)	/	/	/
Lake Consuelo (CON1)	-13.95	-68.991	1360	TERR	Urrego et al. (2005); Urrego et al. (2010)	1	1	1
Lake Malawi	-11.22	34.42	470	TERR	DeBusk (1998)	6	3	3
Lake Masoko	-9.33	33.75	840	TERR	Vincens et al. (2007)	2	0	0
Lake Nojiri	36.831	138.216	657	TERR	Kumon et al. (2009)	8	0	0
Lake Tulane	29.83	-81.95	36	TERR	Grimm et al. (1993); Grimm et al. (2006)	8	1	1
Lake Wangoom LW87 core	-38.35	142.6	100	TERR	Harle et al. (2002)	7	1	1
Lake Xinias	39.05	22.27	500	TERR	Bottema (1979)	8	3	3
Les Echets G	45.9	4.93	267	TERR	de Beaulieu & Reille (1984)	8	0	0
Little Lake	44.16	-123.58	217	TERR	Grigg et al. (2001)	5	0	0
Lynchs Crater	-17.3667	145.7	760	TERR	Kershaw et al. (2007a)	8	2	2
MD01-2421	36.02	141.77	-2224	MARI	Igarashi & Oba (2006); Oba et al. (2006); Aoki et al. (2008)	7	2	0
MD03-2622 Cariaco Basin	10.7061	-65.1691	-877	MARI	González et al. (2008); González and Dupont (2009)	/	/	/
MD04-2845	45.35	-5.22	-4100	MARI	Sánchez Goñi et al. (2008); Daniau et al. (2009)	8	2	2
MD84-629	32.07	34.35	-745	MARI	Cheddadi & Rossignol-Strick (1995)	8	1	1
MD95-2039	40.58	-10.35	-3381	MARI	Roucoux et al. (2001); Roucoux et al. (2005)	8	0	0
MD95-2042	37.8	-10.17	-3148	MARI	Sánchez Goñi et al. (1999); Sánchez Goñi et al. (2000); Daniau et al. (2007); Sánchez Goñi et al. (2008); Sánchez Goñi et al. (2009)	8	0	0
MD95-2043	36.14	-2.621	-1841	MARI	Sánchez Goñi et al. (2002); Fletcher and Sánchez Goñi (2008)	8	0	0
MD99-2331	41.15	-9.68	-2110	MARI	Sánchez Goñi et al. (2005); Naughton et al. (2007); Sánchez Goñi et al. (2008); Naughton et al. (2009)	8	1	1
Megali Limni	39.1025	26.3208	323	TERR	Margari et al. (2007); Margari et al. (2009)	6	1	0
Mfabeni Peatland	-28.1487	32.51867	11	TERR	Finch & Hill (2008)	5	1	1

Nakafurano	43.367	142.433	173	TERR	Igarashi et al. (1993)	2	0	0
Native Companion Lagoon	-27.68	153.41	20	TERR	Petherick et al. (2008a); Petherick et al. (2008b)	6	1	1
Navarrés	39.1	-0.68	225	TERR	Carrión & van Geel (1999)	3	1	0
ODP 1233 C	-41	-74.45	-838	MARI	Lamy et al. (2004); Heusser et al. (2006)	/	/	/
ODP 820	-16.63	146.3	-280	MARI	Moss & Kershaw (2000); Moss & Kershaw (2007)	7	3	3
ODP site 976	36.2	-4.3	-1108	MARI	Nebout et al. (2002); Masson-Delmotte et al. (2005)	8	1	0
ODP1019	41.66	-124.91	989	MARI	Mix et al. (1999); Pisias et al. (2001)	8	2	2
ODP1078C	-11.92	13.4	-426	MARI	Dupont & Behling (2006); Dupont et al. (2008)	/	/	/
ODP893A	34.28	-120.03	-577	MARI	Heusser (1998); Heusser (2000)	8	0	0
Potato Lake	34.45	-111.33	2222	TERR	Anderson (1993)	4	4	4
Rice Lake (Rice Lake 81)	40.3	-123.22	1100	TERR	L. Heusser, unpublished data	/	/	/
Siberia	-17.09	-64.72	2920	TERR	Mourguiart & Ledru (2003)	1	1	1
Stracciaccappa	42.13	12.32	220	TERR	Giardini (2007)	5	1	1
Tagua Tagua	-34.5	-71.16	200	TERR	Heusser (1990)	6	1	0
Taiquemo	-42.17	-73.6	170	TERR	Heusser et al. (1999); Heusser and Heusser (2006)	8	0	0
Toushe Basin	23.82	120.88	650	TERR	Liew et al. (2006)	8	0	0
Tswaing Crater	-25.4	28.08	1100	TERR	Partridge et al. (1997); Scott et al. (2008); L. Scott, unpublished data;	6	1	1
Tyrrendara Swamp	-38.1986	141.7626	13	TERR	Builth et al. (2008)	/	/	/
Valle di Castiglione	41.9	12.76	44	TERR	Alessio et al. (1986); Follieri et al. (1988); Follieri et al. (1989); Narcisi et al. (1992); Narcisi (1999); Magri & Tzedakis (2000); Magri (2008)	7	2	2
W8709-13 PC	42.11	-125.75	-2712	MARI	Pisias et al. (2001)	7	2	2
W8709-8 PC	42.26	-127.68	-3111	MARI	Heusser (1998); Lyle et al. (1992)	/	/	/
Walker Lake	35.38	-111.71	2500	TERR	Berry et al. (1982); Adam et al. (1985); Hevly (1985)	/	/	/

586

587

588 Table 2. Leave-out cross-validation (with geographically and climatically close sites removed)
 589 using fxTWA-PLSv2 for mean temperature of the coldest month (MTCO), mean temperature
 590 of the warmest month (MTWA) and plant-available water (α) with P-splines smoothed fx
 591 estimation and bins of 0.02, 0.02 and 0.002, respectively. n is the number of components where
 592 the last significant number of components is indicated in **bold**. Avg.bias is the average bias;
 593 RMSEP is the root-mean-square error of prediction; and Δ RMSEP is the per cent change of
 594 RMSEP, which is $100 \times (\text{RMSEP}_n - \text{RMSEP}_{n-1})/\text{RMSEP}_{n-1}$; when $n = 1$, RMSEP_0 is the
 595 RMSEP of the null model. p assesses whether using the current number of components is
 596 significantly different from using one component less. The degree of overall compression is
 597 assessed by linear regression of the cross-validated reconstructions on to the climate
 598 variable; b_1 and $b_{1.se}$ are the slope and the standard error of the slope, respectively. The closer
 599 the slope (b_1) is to 1, the less the compression.

	n	R^2	Avg.bias	RMSEP	Δ RMSEP	p	b_1	$b_{1.se}$
MTCO (°C)	1	0.72	-1.11	6.83	-45.45	0.001	0.83	0.00
	2	0.74	-1.21	6.68	-2.25	0.001	0.84	0.00
	3	0.75	-1.10	6.51	-2.48	0.001	0.85	0.00
	4	0.75	-1.10	6.54	0.53	1.000	0.85	0.00
	5	0.75	-1.13	6.54	-0.07	0.188	0.85	0.00
MTWA (°C)	1	0.54	-0.33	3.89	-29.76	0.001	0.66	0.00
	2	0.58	-0.32	3.69	-5.10	0.001	0.71	0.00
	3	0.59	-0.33	3.68	-0.14	0.001	0.71	0.00
	4	0.59	-0.33	3.69	0.07	0.746	0.71	0.00
	5	0.59	-0.33	3.67	-0.39	0.001	0.71	0.00
α	1	0.62	-0.02	0.189	-37.73	0.001	0.66	0.00
	2	0.63	-0.022	0.188	-0.81	0.001	0.68	0.00
	3	0.63	-0.021	0.186	-0.87	0.001	0.68	0.00
	4	0.65	-0.02	0.182	-2.11	0.001	0.71	0.00
	5	0.65	-0.02	0.182	0.11	1.000	0.71	0.00

600 Table 3: Maximum likelihood estimates of the relationship between the change in mean
 601 temperature of the coldest month (ΔMTCO) and the change in mean temperature of the
 602 warmest month (ΔMTWA) by latitudinal bands for the northern extratropics (NET, north of
 603 23.5°N), tropics (TROP, between 23.5°N and 23.5°S) and southern extratropics (SET, south of
 604 23.5°S). The intercepts were set to zero since both variables are changes. Coefficients in bold
 605 mean both the lower 95% and upper 95% estimates are above 0.

Region		Coefficient	Standard error (SE)	Lower 95%	Upper 95%
NET	Slope	2.055	0.257	1.551	2.560
TROP	Slope	0.983	0.551	-0.098	2.064
SET	Slope	1.849	0.772	0.336	3.363

606

607

608 Table 4: Maximum likelihood estimates of the relationship between the change in plant-
 609 available water ($\Delta\alpha$) and the change in mean temperature of the warmest month (ΔMTWA) by
 610 latitudinal bands for the northern extratropics (NET, north of 23.5°N), tropics (TROP, between
 611 23.5°N and 23.5°S) and southern extratropics (SET, south of 23.5°S). The intercepts were set
 612 to zero since both variables are changes. Coefficients in bold mean both the lower 95% and
 613 upper 95% estimates are above 0.

Region		Coefficient	Standard error (SE)	Lower 95%	Upper 95%
NET	Slope	0.066	0.009	0.048	0.084
TROP	Slope	0.059	0.020	0.019	0.098
SET	Slope	0.071	0.020	0.032	0.110

614